Electronic Supplementary Information to "Interaction- and phonon-induced topological phase transitions in double helical liquids"

Chen-Hsuan Hsu

Institute of Physics, Academia Sinica, Taipei 11529, Taiwan

CONTENTS

I. Details about the model and the setup

In this section we present details about the bosonized model and the setup discussed in the main text. In the original fermionic expression, the local and nonlocal pairing terms induced by the proximity effect are given by [S1–S3]

$$V_{\text{loc}} = \sum_{n=1,2} \int dr \left[\frac{\Delta_n}{2} (\psi_{R,n}^\dagger \psi_{L,n}^\dagger - \psi_{L,n}^\dagger \psi_{R,n}^\dagger) + \text{H.c.} \right], \tag{S1}$$

$$V_{\text{cap}} = \int dr \left[\frac{\Delta_c}{2} (\psi_{R,1}^\dagger \psi_{L,2}^\dagger - \psi_{L,2}^\dagger \psi_{R,1}^\dagger) + (1 \leftrightarrow 2) \right] + \text{H.c.}, \tag{S2}$$

with the fermion field $\psi_{\ell,n}$ defined in the main text, and the local (Δ_n) and nonlocal (Δ_c) pairing strengths. These terms can be bosonized into Eqs. (4) and (5) in the main text. When converting to the symmetric/antisymmetric ($\delta \in \{s, a\}$) basis, we introduce the parameters $\Delta_\pm = (\Delta_1 \pm \Delta_2)/2$ and organize the local pairing terms into two parts, $V_{\text{loc}} = V_{\text{loc},+} + V_{\text{loc},-}$, with

$$V_{\text{loc},+} = \int dr \, \frac{2\Delta_+}{\pi a} \cos(\sqrt{2}m\theta_s) \cos(\sqrt{2}m\theta_a), \tag{S3}$$

$$V_{\text{loc},-} = -\int dr \, \frac{2\Delta_-}{\pi a} \sin(\sqrt{2}m\theta_s) \sin(\sqrt{2}m\theta_a). \tag{S4}$$

In general, these cosine terms cannot be directly diagonalized. We thus perform perturbative renormalization-group (RG) analysis on these pairing terms. Below we specify the setup and the corresponding parameter regime suitable for our analysis, and demonstrate the emergence of the self-dual sine-Gordon model from the system.

I A. Identical pairing setup

In the main text we consider the identical pairing setup with $\Delta_1 = \Delta_2$, such that $\Delta_- = 0$. In this case, the electronic subsystem is described by

$$H_{\text{dh}} + V_{\text{loc}} + V_{\text{cap}} = \sum_\delta \int dr \, \frac{\hbar u_\delta}{2\pi} \left[\frac{1}{K_\delta} (\partial_r \phi_\delta)^2 + K_\delta (\partial_r \theta_\delta)^2 \right]$$

$$+ \frac{2}{\pi a} \int dr \, \cos(\sqrt{2}m\theta_s) \left[\Delta_+ \cos(\sqrt{2}m\theta_a) + \Delta_c \cos(\sqrt{2}m\phi_a) \right]. \tag{S5}$$

For $m = 2$, the expression described above can be mapped into the low-energy effective theory of a two-leg spin ladder system [S4, S5], despite the very different physical systems involved. When the θ_s field is frozen, the remaining gapless sector with $\delta = a$ can be recast into the self-dual sine-Gordon model, as stated in the main text and detailed below.

I B. π-junction setup

Alternatively, one may consider the π-junction setup with $\Delta_+ = 0$ but finite Δ_- [S2, S6, S7]. This alternative setup can also fulfill the topological criterion in Eq. (6) in the main text. Interestingly, by performing a shift in $\theta_s \to \theta_s + \pi/(4\sqrt{2}m)$ and $\theta_a \to \theta_a + 3\pi/(2\sqrt{2}m)$, we obtain

$$V_{\text{loc}} + V_{\text{cap}} \to \frac{\sqrt{2}}{\pi a} \int dr \, \langle \cos(\sqrt{2}m\theta_s) \rangle \left[\Delta_- \cos(\sqrt{2}m\theta_a) + \Delta_c \cos(\sqrt{2}m\phi_a) \right], \tag{S6}$$

where we have assumed a frozen θ_s field with $\langle \cos(\sqrt{2}m\theta_s) \rangle \to 1$ and thus $\langle \sin(\sqrt{2}m\theta_s) \rangle \to 0$. Therefore, we recover the self-dual sine-Gordon model from the π-junction setup, with different effective parameters.

I C. Self-dual sine-Gordon model

Here we demonstrate that, with either identical pairing or π-junction setup introduced above, we can obtain the self-dual sine-Gordon model when the symmetric sector is gapped. Starting with Eq. (S5) and assuming that the θ_s field is frozen, we get

$$H_{\text{dh}} + V_{\text{loc}} + V_{\text{cap}} = \int dr \, \frac{\hbar u_a}{2\pi} \left[\frac{1}{K_a} \left(\partial_r \phi_a \right)^2 + K_a \left(\partial_r \theta_a \right)^2 \right]$$
$$+ \frac{2}{\pi a} \int dr \, \langle \cos(\sqrt{2}m\theta_s) \rangle \left[\Delta_+ \cos(\sqrt{2}m\theta_a) + \Delta_c \cos(\sqrt{2}m\phi_a) \right]. \tag{S7}$$

Introducing a new set of boson fields, $\Phi = \sqrt{m/(\pi K_a)}\phi_a$ and $\Theta = \sqrt{mK_a/\pi}\theta_a$, we have

$$[\Phi(r), \Theta(r')] = \frac{i\pi}{2}\text{sign}(r' - r). \tag{S8}$$

The remaining, gapless sector is then

$$H_{\text{dh}} + V_{\text{loc}} + V_{\text{cap}} = \int dr \, \frac{\hbar u}{2} \left[\left(\partial_r \Phi \right)^2 + \left(\partial_r \Theta \right)^2 \right] + \int \frac{dr}{a} \left[g_\phi \cos(\lambda_\phi \Phi) + g_\theta \cos(\lambda_\theta \Theta) \right], \tag{S9}$$

with $u = u_a/m$, $g_\phi = (2\Delta_c/\pi)\langle\cos(\sqrt{2}m\theta_s)\rangle$, $g_\theta = (2\Delta_+/\pi)\langle\cos(\sqrt{2}m\theta_s)\rangle$, $\lambda_\phi = \sqrt{2\pi mK_a}$, and $\lambda_\theta = \sqrt{2\pi m/K_a}$. The perturbation part in the above expression is presented in Eq. (7) in the main text.

We therefore obtain the self-dual sine-Gordon model, as in Ref. [S8]. At the self-duality point $K_a(l^*) = 1$, we observe a hierarchy of self-dual sine-Gordon models characterized by different m values, with each class described by $\lambda_\phi^2 = \lambda_\theta^2 = 2\pi m$ [S8]. Limiting the choice of m to odd integers, which correspond to a time-reversal-invariant generalization of Laughlin states at the fractional filling $\nu = 1/m$, would directly recover the fermion anticommutator of the original electron operators [S1]. However, motivated by observations that indicated fractional quantum spin Hall states corresponding to a time-reversal pair of *even-denominator* fractional Chern insulating states, we opt to keep a general m. Remarkably, the tunability of two-dimensional topological materials, including twisted bilayer systems, could serve as a versatile platform for exploring the model for distinct m [S9–S11], including the fractional helical liquid regime.

The critical behaviors of the $2\pi m$ self-dual sine-Gordon models have been widely explored in the literature [S8, S12, S13], featuring Z_2 Ising criticality for $m = 2$ and Z_4 parafermion theory for $m = 3$ with three-state Potts universality. Furthermore, while the leading-order RG analysis suggested the irrelevance of the model with $m > 4$, the model with a higher m value can be stabilized when including the third-order RG contribution [S8, S12, S13]. Nevertheless, our focus is not on the critical behaviors at the self-duality point, but rather on the topological properties of the g_ϕ- and g_θ-dominated phases.

To further explore the phase competition between the g_ϕ- and g_θ-dominated phases, we refermionize the above expression for $m = 2$. With $\Psi_\ell = e^{\sqrt{\pi}i(-\ell\Phi+\Theta)}$ for $\ell \in \{R, L\}$, we get

$$V_{\text{loc}} + V_{\text{cap}} = \int \frac{dr}{2a} \left[g_\phi \Psi_R^\dagger \Psi_L + g_\theta \Psi_R \Psi_L + h.c. \right]. \tag{S10}$$

To proceed, we introduce Majorana fields ξ_ℓ and η_ℓ related to the field $\Psi_\ell = (\xi_\ell + i\eta_\ell)/\sqrt{2}$, and obtain

$$V_{\text{loc}} + V_{\text{cap}} = i \int \frac{dr}{2a} \left[(g_\phi + g_\theta)\xi_R\eta_L + (g_\theta - g_\phi)\eta_R\xi_L \right], \tag{S11}$$

which is given in Eq. (8) in the main text. The Majorana representation provides an alternative, useful way in establishing the topological phase transition from the competition between the g_ϕ and g_θ terms.

I D. Electrical tunability of the setup

In this section we estimate the intrachannel and interchannel interaction strengths in our setup shown in Fig. 1 in the main text, following Refs. [S2, S14, S15]. For the intrachannel interaction strength, we have $U_{ee} \approx \frac{e^2}{\pi\epsilon} \ln\left[\frac{D_{sc}}{\min(\xi,d)}\right]$, with the Fermi velocity v_F and the decay length ξ of the helical states, the dielectric constant ϵ of the host material, and the screening length D_{sc} from a nearby metallic gate [S2, S14]. For the interchannel interaction strength, we consider the screened Coulomb potential between two parallel channels separated by a distance d with a dielectric layer and compute it numerically following a similar approach for emergent parallel one-dimensional channels in twisted bilayer systems [S15].

In Fig. S1, we illustrate the intrachannel strength in Panel (a) and the ratio between the interchannel and intrachannel strengths in Panel (b). The intrachannel strength can be modulated through the screening effect, which is controlled by either the distance between the channel and the metallic gate or the choice of the dielectric material. As the interchannel strength also depends on the distance between the two channels, the interlayer separation d and the dielectric constant ϵ' of the material between the two layers offer additional knobs to adjust the V_{ee}/U_{ee} ratio. This estimation demonstrates the electrical tunability of the system, which can be used to induce a topological phase transition discussed in the main text.
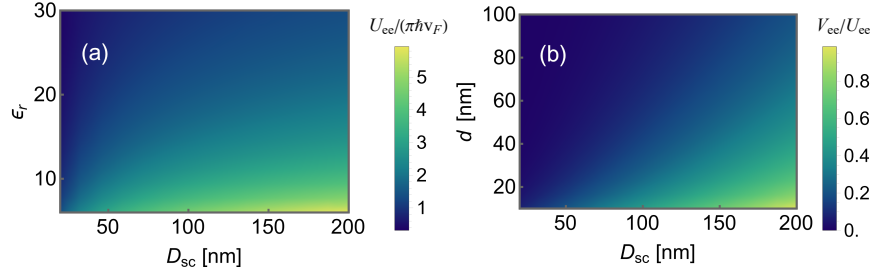

FIG. S1. (a) Intrachannel interaction strength U_{ee} as a function of the screening length D_{sc} and the relative permittivity $\epsilon_r = \epsilon/\epsilon_0$ of the dielectric material, where ϵ_0 is the vacuum dielectric constant. The additional parameters are $v_F = 2 \times 10^5$ m/s and $\xi = 10$ nm. (b) Ratio of interchannel-to-intrachannel strength V_{ee}/U_{ee} as a function of the screening length D_{sc} and the interlayer separation d. Here, the relative permittivity $\epsilon'_r = 6.6$ of the materials between the two (fractional) quantum spin Hall layers corresponds to hexagonal boron nitride, with other parameters the same as those in Panel (a).

II. Operator product expansion

In this section we present useful formulas for the operator product expansion (OPE) procedure. For notational simplicity, we assume $m = 1$ and absence of phonons for now, which give

$$\langle [\phi_\delta(r_1, \tau_1) - \phi_\delta(r_2, \tau_2)]^2 \rangle = K_\delta \ln(|\mathbf{r}|/a), \tag{S12a}$$

$$\langle [\theta_\delta(r_1, \tau_1) - \theta_\delta(r_2, \tau_2)]^2 \rangle = \frac{1}{K_\delta} \ln(|\mathbf{r}|/a), \tag{S12b}$$

with the coordinate (r_j, τ_j), the average $\langle \cdots \rangle$ with respect to the electronic action, and $|\mathbf{r}| = \sqrt{(r_1 - r_2)^2 + (u_\delta|\tau_1 - \tau_2| + a)^2}$. In terms of the coordinate $z_j = -ir_j + u_\delta\tau_j$ and its complex conjugate $\bar{z}_j$, we have

$$\langle \phi_\delta(z_1, \bar{z}_1)\phi_\delta(z_2, \bar{z}_2) \rangle = \frac{K_\delta}{2} \ln\left|\frac{L}{z}\right|, \tag{S13a}$$

$$\langle \theta_\delta(z_1, \bar{z}_1)\theta_\delta(z_2, \bar{z}_2) \rangle = \frac{1}{2K_\delta} \ln\left|\frac{L}{z}\right|. \tag{S13b}$$

We define the following operators,

$$J_{\phi_\delta} = i\,\partial_z\phi_\delta(z, \bar{z})|_{(z,\bar{z})\to(Z,\bar{Z})}\,, \quad \bar{J}_{\phi_\delta} = -i\,\partial_{\bar{z}}\phi_\delta(z, \bar{z})|_{(z,\bar{z})\to(Z,\bar{Z})}\,, \tag{S14a}$$

$$J_{\theta_\delta} = i\,\partial_z\theta_\delta(z, \bar{z})|_{(z,\bar{z})\to(Z,\bar{Z})}\,, \quad \bar{J}_{\theta_\delta} = -i\,\partial_{\bar{z}}\theta_\delta(z, \bar{z})|_{(z,\bar{z})\to(Z,\bar{Z})}\,, \tag{S14b}$$

with the derivative $\partial_z = \frac{1}{2}\left(\frac{1}{u}\partial_\tau + i\partial_r\right)$, its complex conjugate $\partial_{\bar{z}}$, $Z = (z_1 + z_2)/2$ and its complex conjugate $\bar{Z}$.
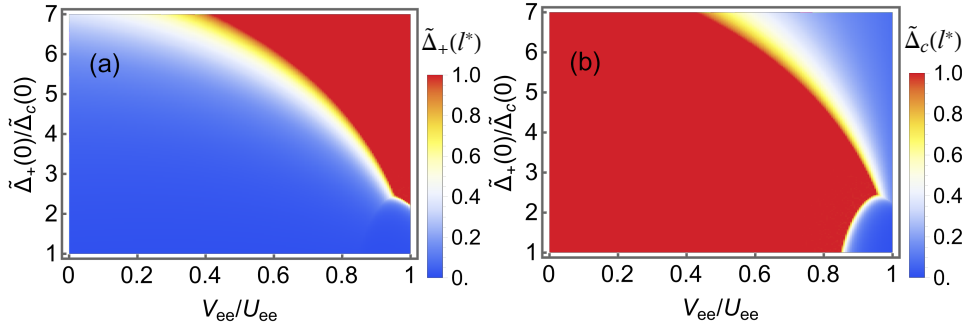
FIG. S2. Renormalized pairing strengths, obtained from the RG flows and used to determine the phase diagram in Fig. 2 in the main text. The region where neither $\tilde{\Delta}_+$ nor $\tilde{\Delta}_c$ reaches unity is marked as "DH" (for "double helical liquid") in Fig. 2. The adopted values for the other parameters are $\tilde{\Delta}_c(0) = 0.03$ and $U_{ee}/(\pi \hbar v_F) = 2.5$.

With the above formulas, the quadratic terms are

$$J_{\phi_\delta} \bar{J}_{\phi_\delta} = \frac{1}{4} \left(|\partial_R \phi_\delta|^2 + \frac{1}{u_\delta^2} |\partial_T \phi_\delta|^2 \right), \tag{S15a}$$

$$J_{\theta_\delta} \bar{J}_{\theta_\delta} = \frac{1}{4} \left(|\partial_R \theta_\delta|^2 + \frac{1}{u_\delta^2} |\partial_T \theta_\delta|^2 \right), \tag{S15b}$$

with $R = (r_1 + r_2)/2$ and $T = (t_1 + t_2)/2$.

Using $e^A e^B =: e^{A+B} : e^{\langle AB + \frac{A^2+B^2}{2} \rangle}$ for two boson fields A and B whose commutator is a complex number, we write down the OPE formulas [S16, S17]. For the sector δ, we get

$$e^{i\lambda \phi_\delta(z_1, \bar{z}_1)} e^{-i\lambda \phi_\delta(z_2, \bar{z}_2)} + (\lambda \to -\lambda) = \frac{2}{\left(|z|/a \right)^{\lambda^2 K_\delta/2}} \left(1 - \lambda^2 |z|^2 : J_{\phi_\delta} \bar{J}_{\phi_\delta} : + \cdots \right), \tag{S16a}$$

$$e^{i\lambda \theta_\delta(z_1, \bar{z}_1)} e^{-i\lambda \theta_\delta(z_2, \bar{z}_2)} + (\lambda \to -\lambda) = \frac{2}{\left(|z|/a \right)^{\lambda^2/(2K_\delta)}} \left(1 - \lambda^2 |z|^2 : J_{\theta_\delta} \bar{J}_{\theta_\delta} : + \cdots \right), \tag{S16b}$$

which are used to derive the RG flow equations.

In the absence of phonons, we obtain the following equations for the RG flow for general m,

$$\frac{d\tilde{\Delta}_+}{dl} = \left[2 - \frac{m}{2} \left(\frac{1}{K_s} + \frac{1}{K_a} \right) \right] \tilde{\Delta}_+, \tag{S17a}$$

$$\frac{d\tilde{\Delta}_c}{dl} = \left[2 - \frac{m}{2} \left(\frac{1}{K_s} + K_a \right) \right] \tilde{\Delta}_c, \tag{S17b}$$

$$\frac{dK_s}{dl} = 2m\tilde{\Delta}_+^2 + 2m\tilde{\Delta}_c^2, \tag{S17c}$$

$$\frac{dK_a}{dl} = 2m\tilde{\Delta}_+^2 - 2mK_a^2\tilde{\Delta}_c^2. \tag{S17d}$$

The presence of phonons modifies the RG flow equations, which we present in Eq. (13) in the main text.

The set of differential equations in Eq. (S17) are numerically solved. An example of the RG flow diagram without the influence of phonons is displayed in Fig. 2 in the main text, along with the corresponding phase diagram and the renormalized values of the interaction parameters. In Fig. S2, we additionally present the renormalized values of the pairing strengths extracted at the end of the RG flows, from which we deduce the phase diagram.

III. Phonon influence

In this section, we discuss the influence of phonons on the double helical liquid. We first present the action $S_{\text{ee}} + S_{\text{ph}} + S_{\text{ep}}$ for the unperturbed system. For the electronic part, we have

$$S_{\text{ee}} = \sum_{\delta} \frac{\hbar}{2\pi} \int dr d\tau \left[-\frac{2i}{m} \partial_r \theta_\delta \partial_\tau \phi_\delta + \frac{u_\delta}{K_\delta} \left(\partial_r \phi_\delta \right)^2 + u_\delta K_\delta \left(\partial_r \theta_\delta \right)^2 \right], \tag{S18}$$

with the imaginary time τ. In addition, the contributions involving phonons can be written as [S15, S18, S19]

$$S_{\text{ph}} + S_{\text{ep}} = \sum_n \int dr d\tau \left\{ -i\pi_n \partial_\tau d_n + \frac{1}{2\rho} \left[\pi_n^2 + \rho^2 c^2 \left(\partial_r d_n \right)^2 \right] + g \partial_r \phi_n \partial_r d_n \right\}, \tag{S19}$$

derived from Eqs. (9) and (10) in the main text.

Upon expressing the electron fields in the s/a basis and integrating out the phonon fields, we obtain the effective action,

$$S_{\text{ee}} + S_{\text{ph}} + S_{\text{ep}} \rightarrow S_{\text{eff}} = \frac{1}{2\beta L} \sum_\delta \sum_{\omega_n, q} \left[\frac{\omega_n^2 + u_\delta^2 q^2}{\pi u_\delta K_\delta} - \frac{g^2 q^4 / (\rho \hbar)}{\omega_n^2 + c^2 q^2} \right] |\phi_\delta (\omega_n, q)|^2, \tag{S20}$$

from which we deduce excitation modes with the velocities given in Eq. (11) in the main text. The effective action remains quadratic in the bosonic fields, enabling nonperturbative calculations at all orders of g, in contrast to perturbative analysis that retain terms only up to a certain order of g.

Concerning the RG flow, the primary effect from the phonons is to modify the scaling dimensions of the two pairing operators in Eqs. (4) and (5). In the presence of phonons, the scaling dimensions corresponding to the Δ_+ and Δ_c terms become

$$d_+ = \frac{m}{2} \sum_{\eta=\pm} \left(\frac{u_s \gamma_{s,\eta}^\theta}{K_s u_{s,\eta}} + \frac{u_a \gamma_{a,\eta}^\theta}{K_a u_{a,\eta}} \right), \tag{S21}$$

$$d_c = \frac{m}{2} \sum_{\eta=\pm} \left(\frac{u_s \gamma_{s,\eta}^\theta}{K_s u_{s,\eta}} + \frac{u_a K_a \gamma_{a,\eta}^\phi}{u_{a,\eta}} \right), \tag{S22}$$

which enter the RG flow equations (13) in the main text. Since we consider the RG contributions only up to the second order in the perturbation strengths $\tilde{\Delta}_+$ and $\tilde{\Delta}_c$, the phonon-related parameters, such as c and g, are not renormailzed at this order.

IV. More numerical results from the RG analysis

In this section, we present more numerical results from our RG analysis.

IV A. Additional results for different initial values for the pairing strengths

Here we discuss the numerical results for different initial values for the pairing gap ratio of $\tilde{\Delta}_+(0)/\tilde{\Delta}_c(0)$. In Fig. S3, we display additional RG flow and phase diagrams for $U_{ee}/(\pi \hbar v_F) = 2.5$ and $\tilde{\Delta}_c(0) = 0.03$, corresponding to Figs. 2 and 4 in the main text.

For a detailed examination, additional RG flows IIIa and IIIb are displayed in Fig. S3(a,b), showing overlapped plots for flows with and without the influence of phonons. As discussed in the main text, under the RG flow, K_a is renormalized to a larger value in the presence of phonons, thereby favoring the ordering of θ_a and promoting local pairing. Consequently, a sufficiently strong electron-phonon coupling drives the system into a topologically trivial state.

From Fig. 4 in the main text and Fig. S3(c–e) here, we observe the overall trend upon varying the ratio $\tilde{\Delta}_+(0)/\tilde{\Delta}_c(0)$. Namely, with a larger initial ratio of $\tilde{\Delta}_+(0)/\tilde{\Delta}_c(0)$, a smaller V_{ee}/U_{ee} ratio is needed to suppress nonlocal pairing. Consequently, the system transits into a trivial phase in the presence of a weaker interchannel interaction and electron-phonon coupling, confirming our conclusion in the main text. Additionally, with the phonon influence, the regime beyond the Wentzel-Bardeen (WB) singularity is reached for a sufficiently large v_g and V_{ee}.
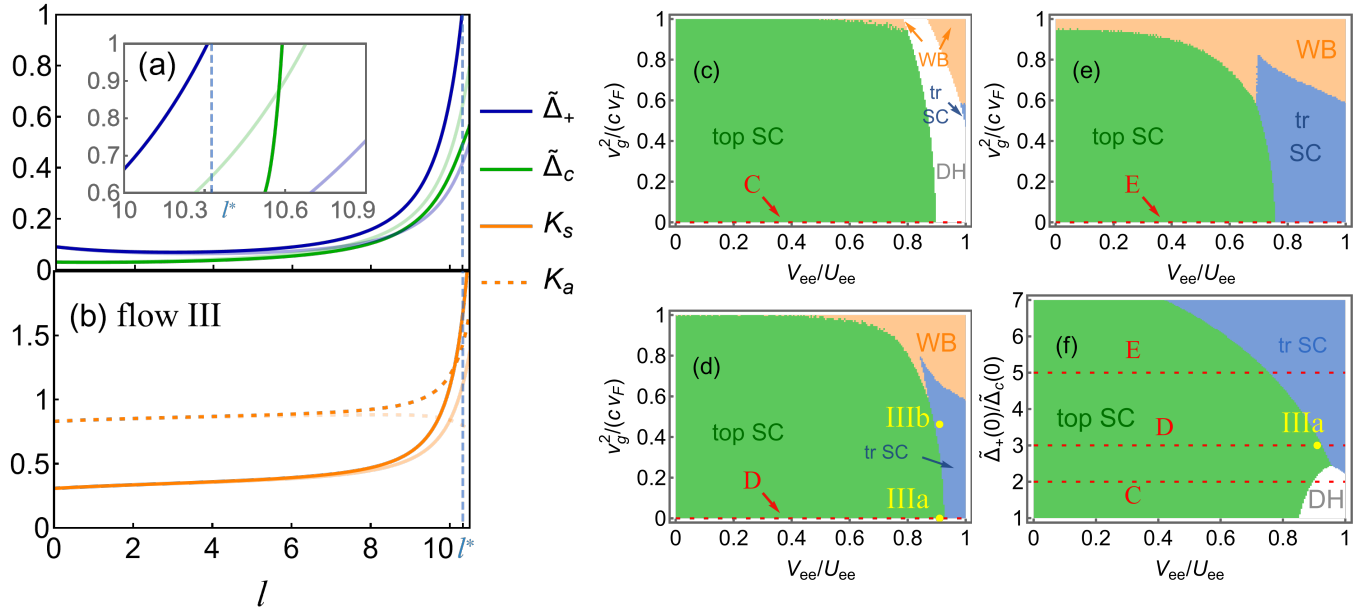
FIG. S3. Additional RG flow and phase diagrams for $U_{ee}/(\pi\hbar v_F) = 2.5$ and $\tilde{\Delta}_c(0) = 0.03$, corresponding to Figs. 2 and 4 in the main text. (a,b) RG flows with $\tilde{\Delta}_+(0) = 0.09$ and $V_{ee}/U_{ee} = 0.9$. For a direct comparison, the flows with and without phonons are plotted together, with the latter in dimmer colors. The former is with $v_g^2/(cv_F) = 0.42$. The inset shows a zoom-in region close to the end point of the flow. (c–e) Phase diagrams for (c) $\tilde{\Delta}_+(0) = 0.06$, (d) $\tilde{\Delta}_+(0) = 0.09$, and (e) $\tilde{\Delta}_+(0) = 0.15$. (f) Phase diagram without the phonon contribution, identical to Fig. 2(b), but with new labels for the dot and line cuts corresponding to Panels (a–e).

IV B. Additional results for different intrachannel interaction strength

Next, we present additional RG results to demonstrate that our conclusion holds for a different intrachannel interaction strength. We show results without phonon contribution in Fig. S4 (corresponding to Fig. 2 in the main text) and include phonon contribution in Fig. S5 (corresponding to Fig. 4 in the main text). Compared to the main text, here we choose a weaker intrachannel interaction and hence a stronger tendency towards local pairing, leading to a more balanced competition between topological and trivial superconductivity. We again obtain rich phase diagrams incorporating trivial and topological superconductivity, gapless double helical liquids, and a strong electron-phonon-coupled liquid.

From Fig. S4, we see that a topological phase transition can be triggered by the interchannel interaction. Upon adjusting V_{ee}/U_{ee}, the electronic self duality can be reached, with $\Delta_+(l^*) = \Delta_c(l^*)$ in Fig. S4(b) and $K_a(l^*) \to 1$ indicated in Fig. S4(d). In Fig. S5(a,b), we observe a marked difference between the RG flows without and with the phonon contributions, resulting in rich phase diagrams in Fig. S5. In both scenarios, topological phase transitions can occur, driven by either the interchannel interactions, electron-phonon coupling, or combination of the two, further confirming our main conclusion.
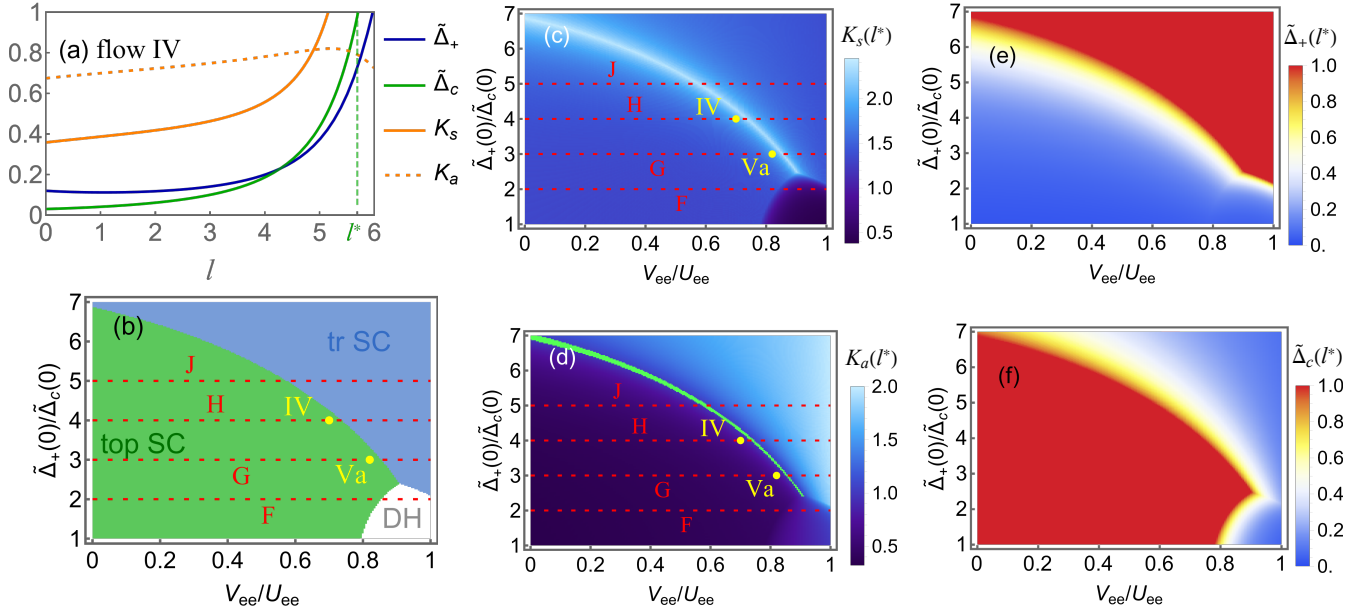
FIG. S4. RG flow and phase diagrams without phonon contribution for $U_{ee}/(\pi\hbar v_F) = 2$ and $\tilde{\Delta}_c(0) = 0.03$. (a) RG flow diagram for $\tilde{\Delta}_+(0) = 0.12$ and $V_{ee}/U_{ee} = 0.7$. (b) Phase diagram for a range of $\tilde{\Delta}_+(0)/\tilde{\Delta}_c(0) \in [1, 7]$ and $V_{ee}/U_{ee} \in [0, 1]$, along with the renormalized values of $K_s(l^*)$ and $K_a(l^*)$ in Panels (c,d) and the renormalized pairing strengths in Panels (e,f). The light green color in Panel (d) highlights the region where K_a flows to unity. The dot IV and line cuts labeled by F, G, H and J correspond to the initial values of the RG flow in Panel (a) here and Panels (c–f) in Fig. S5, respectively.
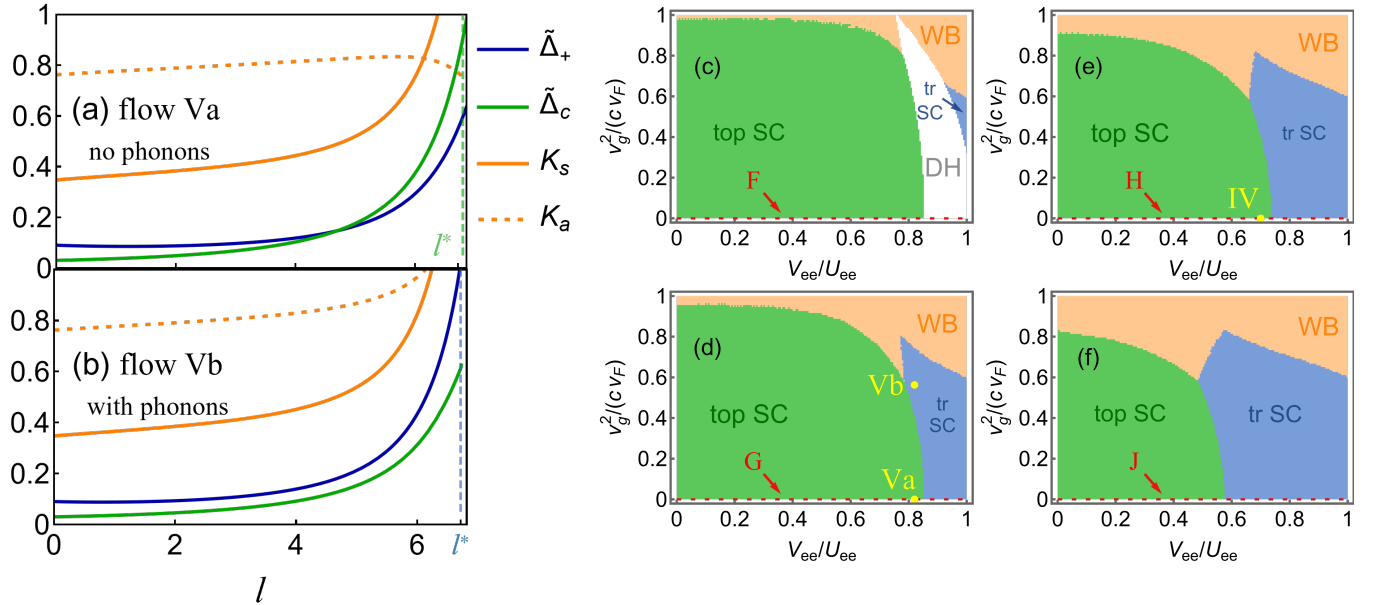

FIG. S5. RG flow and phase diagrams for $U_{ee}/(\pi\hbar v_F) = 2$ and $\tilde{\Delta}_c(0) = 0.03$. (a,b) RG flows for $\tilde{\Delta}_+(0) = 3\tilde{\Delta}_c(0)$, $V_{ee}/(\pi\hbar v_F) = 0.82$ $U_{ee}/(\pi\hbar v_F) = 1.64$ in the (a) absence of phonons and (b) presence of phonons with $v_g^2/(c v_F) = 0.56$. (c–f) Phase diagrams for (c) $\tilde{\Delta}_+(0) = 0.06$, (d) $\tilde{\Delta}_+(0) = 0.09$, (e) $\tilde{\Delta}_+(0) = 0.12$ and (f) $\tilde{\Delta}_+(0) = 0.15$, with the line cuts F, G, H and J corresponding to those in Fig. S4. The two dots in Panel (d) correspond to the initial points of the RG flows Va and Vb in Panels (a,b), and the dot in Panel (e) correspond to Fig. S4(a). The adopted values of the other parameters are the same as those in Fig. S4.

IV C. Results for double fractional helical liquids ($m > 1$)

In the main text and above, we present numerical results for $m = 1$, applicable to double helical liquids in more common integer quantum spin Hall states. Here, in Fig. S6, we extend the analysis to the $m = 2$ case.

In Figs. S6(a,b) and (e,f), we illustrate the RG flows with and without phonon influence, again reaching distinct pairing phases at the end of the RG flow due to the opposite renormalization trends of the K_a parameter. Notably, the stronger renormalization of interaction parameters for $m > 1$ means that even a smaller electron-phonon coupling g is sufficient to drive the phase transition and reach the WB boundary. In addition, compared to the $m = 1$ case above, K_s increases rapidly in both scenarios.

Examples for the phase diagrams are shown in Figs. S6(c,d) and (g,h); here we choose to use U_{ee} for the horizontal axis. The flow of interaction parameters again helps drive the system into the trivial regime. We observe that, in the fractional regime, a more fragile topological phase exists where weaker electron-phonon coupling is necessary to induce the transition. Furthermore, as a result of larger scaling dimensions for both pairing operators, it becomes more difficult for both types of superconductivity to survive, thus enlarging the area for gapless helical liquids, as indicated in Fig. S6(g,h). Finally, with the numerical results presented here, we expect an even more fragile topological superconductivity in fractional helical liquids with a higher m value.
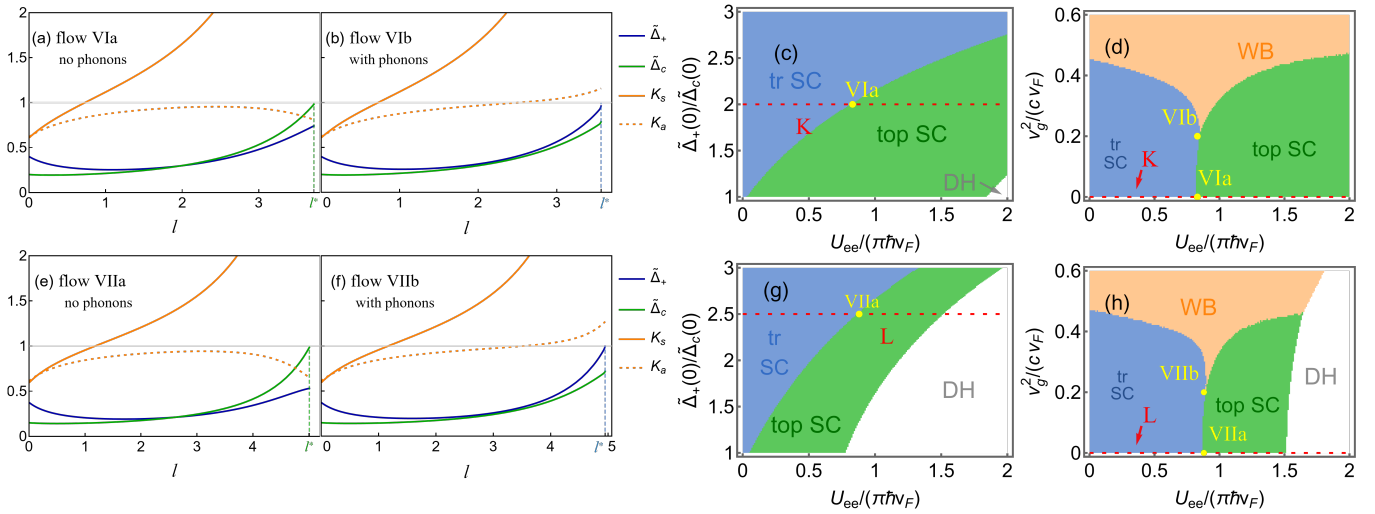

FIG. S6. RG flow and phase diagrams for $m = 2$. (a,b) RG flows for $\tilde{\Delta}_+(0) = 2\tilde{\Delta}_c(0) = 0.4$, $U_{ee}/(\pi \hbar v_F) = 0.83$ and $V_{ee}/(\pi \hbar v_F) = 0.025$ in the (a) absence of phonons and (b) presence of phonons with $v_g^2/(c v_F) = 0.2$. (c) Phase diagram without phonon contribution for $V_{ee}/(\pi \hbar v_F) = 0.03$ and $\tilde{\Delta}_c(0) = 0.2$. (d) Phase diagram with phonon contribution for $V_{ee}/(\pi \hbar v_F) = 0.03$ and $\tilde{\Delta}_+(0) = 2\tilde{\Delta}_c(0) = 0.4$. The line cut K in Panels (c,d) is marked. The dots VIa and VIb in Panels (c,d) correspond to the initial points of the RG flows in Panels (a,b). (e,f) Similar plots to Panels (a,b), but with $\tilde{\Delta}_+(0) = 2.5\tilde{\Delta}_c(0)$, $\tilde{\Delta}_c(0) = 0.15$, $U_{ee}/(\pi \hbar v_F) = 0.88$, $V_{ee}/(\pi \hbar v_F) = 0.05$ and $v_g^2/(c v_F) = 0.2$. (g,h) Similar plots to Panels (c,d), but with $\tilde{\Delta}_+(0) = 2.5\tilde{\Delta}_c(0)$, $\tilde{\Delta}_c(0) = 0.15$, $V_{ee}/(\pi \hbar v_F) = 0.05$ and $v_g^2/(c v_F) = 0.2$. The line cut L in Panels (g,h) is marked. The dots VIIa and VIIb in Panels (g,h) correspond to the initial points of the RG flows in Panels (c,d).

[S1] J. Klinovaja, A. Yacoby, and D. Loss, Phys. Rev. B **90**, 155447 (2014).

[S2] C.-H. Hsu, P. Stano, J. Klinovaja, and D. Loss, Phys. Rev. Lett. **121**, 196801 (2018).

[S3] C.-H. Hsu, P. Stano, J. Klinovaja, and D. Loss, Semicond. Sci. Technol. **36**, 123003 (2021).

[S4] A. Jaefari and E. Fradkin, Phys. Rev. B **85**, 035104 (2012).

[S5] G. Y. Cho, R. Soto-Garrido, and E. Fradkin, Phys. Rev. Lett. **113**, 256405 (2014).

[S6] C. Schrade, M. Thakurathi, C. Reeg, S. Hoffman, J. Klinovaja, and D. Loss, Phys. Rev. B **96**, 035306 (2017).

[S7] K. Laubscher, D. Chughtai, D. Loss, and J. Klinovaja, Phys. Rev. B **102**, 195401 (2020).

[S8] P. Lecheminant, A. O. Gogolin, and A. A. Nersesyan, Nucl. Phys. B **639**, 502 (2002).

[S9] K. Kang, B. Shen, Y. Qiu, Y. Zeng, Z. Xia, K. Watanabe, T. Taniguchi, J. Shan, and K. F. Mak, Nature **628**, 522 (2024).

[S10] K. Kang, Y. Qiu, K. Watanabe, T. Taniguchi, J. Shan, and K. F. Mak, Observation of the double quantum spin Hall phase in moiré WSe$_2$ (2024), arXiv:2402.04196 [cond-mat.mes-hall].

[S11] J. Tang, T. S. Ding, H. Chen, A. Gao, T. Qian, Z. Huang, Z. Sun, X. Han, A. Strasser, J. Li, M. Geiwitz, M. Shehabeldin, V. Belosevich, Z. Wang, Y. Wang, K. Watanabe, T. Taniguchi, D. C. Bell, Z. Wang, L. Fu, Y. Zhang, X. Qian, K. S. Burch, Y. Shi, N. Ni, G. Chang, S.-Y. Xu, and Q. Ma, Nature **628**, 515 (2024).

[S12] D. Boyanovsky, J. Phys. A: Math. Gen. **22**, 2601 (1989).

[S13] E. Sagi, A. Haim, E. Berg, F. von Oppen, and Y. Oreg, Phys. Rev. B **96**, 235144 (2017).

[S14] J. Maciejko, C. Liu, Y. Oreg, X.-L. Qi, C. Wu, and S.-C. Zhang, Phys. Rev. Lett. **102**, 256803 (2009).

[S15] H.-C. Wang and C.-H. Hsu, 2D Mater. **11**, 035007 (2024).

[S16] J. von Delft and H. Schoeller, Ann. Phys. **7**, 225 (1998).

[S17] D. Sénéchal, Theoretical Methods for Strongly Correlated Electrons (Springer New York, NY, 2003) Chap. 4. An Introduction to Bosonization, p. 139.

[S18] D. Loss and T. Martin, Phys. Rev. B **50**, 12160 (1994).

[S19] T. Martin and D. Loss, Int. J. Mod. Phys. B **09**, 495 (1995)